PHYSICAL REVIEW D VOLUME 36, NUMBER 9 1 NOVEMBER 1987

Hadron spectrum on an $18^3 \times 42$ lattice

Rajan Gupta
MS-B285, Los Alamos National Laboratory, Los Alamos, New Mexico 87545

Gerald Guralnik
Physics Department, Brown University, Providence, Rhode Island 02912

Gregory Kilcup
Newman Laboratory of Physics, Cornell University, Ithaca, New York 14853

Apoorva Patel
Physics Department, University of Wuppertal, D-5600 Wuppertal 1, West Germany

Stephen R. Sharpe
Stanford Linear Accelerator Center, Stanford University, Stanford, California 94305

Tony Warnock
Cray Research Inc., Los Alamos, New Mexico 87544
(Received 4 June 1987)

We present results for the hadron spectrum of quenched lattice QCD on an $18^3 \times 42$ lattice at $\beta = 6.2$. We compare $r = \frac{1}{2}$ Wilson fermions with quark masses in the range $m_q/m_s = 1$ to 5 to staggered fermions with $m_q/m_s = \frac{1}{3}$ to 2. In the overlap region we find that the spectra agree, and that both yield $a^{-1} \approx 2.5$ GeV, if we use m_ρ to set the scale. We also find that the flavor symmetry of the staggered fermions is restored to a greater degree than at lower β. However, for both types of fermion, the nucleon to ρ mass ratio comes out too high, never dipping below 1.5. We show the advantages to be gained with staggered fermions by using operators nonlocal in time. Using these operators we uncover a second problem: an anomalously light flavor-nonsinglet scalar. We also present results for the $\pi^+ - \pi^0$ electromagnetic mass splitting and for the Landau-gauge gluon propagator.

I. INTRODUCTION

The hadron spectrum in the quenched approximation is an obvious benchmark which must be established before lattice methods can be usefully applied to less straightforward problems of QCD. *A priori* we should not expect to get physically correct answers from this drastic approximation, yet it is important to pin down the predictions of the quenched model before investing in the computer time needed to simulate full QCD. Optimistically, if the errors introduced by neglecting fermion loops are understood and shown to be reasonably small, we might trust quenched calculations of more exotic observables such as the nucleon σ term.

The endeavor to extract the quenched spectrum[1-3] is now some five years old, and has proven to be literally orders of magnitude harder than it seemed at first. The lattices used to date have been both too coarse and too small. Present calculations have not yet demonstrated that we have reached the asymptotic scaling regime, or the finite-size scaling regime. That the lattices used so far are too coarse is indicated by studies of the β function of the quenched theory. Monte Carlo renormalization-group studies[4,5] suggest that one may have to use $\beta \equiv 6/g^2 \geq 6.2$ or even $\beta \geq 7.0$ in order to see universal asymptotic scaling. Similarly, the calculation of T_c (Refs. 6 and 7) shows a lack of asymptotic scaling below $\beta = 6.15$. Existing spectrum calculations have primarily explored the region $\beta \leq 6.0$, though preliminary results at $\beta = 6.15$ have been reported by Bowler *et al.*[8]

The second limit one must take is to enlarge the box until the masses follow the asymptotic finite-size scaling formulas.[9] The physical requirement for calculating hadronic observables is that the box be large compared to the pion Compton wavelength at the quark mass used. For the physical pion ($1/m_\pi \approx 1.4$ F) this is the same size as typical lattices in today's computations. Thus even if current β's turn out to be close to the scaling regime, we are still studying QCD in a small box. Much larger lattices are required to simulate hadrons in the physical vacuum.

This paper presents results for the quenched spectrum on a $18^3 \times 42$ lattice, with coupling $\beta = 6.2$, using both Wilson fermions (WF's) and staggered fermions (SF's). This is the weakest coupling used to date, and we have necessarily had to use a very large number of lattice points in order to keep the physical volume roughly the same as that in calculations at smaller β. Thus we are pushing toward the asymptotic scaling limit, but not toward the finite-size scaling limit. We have used a large

sample of configurations, and for SF's we have pushed the quark mass as low as finite-size effects allow. We have also taken considerable effort to obtain reliable statistical errors. Despite this, we do not consider this study to be definitive for the reasons listed above. We merely offer the next data point, and await the next generation of computers to extract the true scaling predictions of the quenched model.

For staggered fermions this calculation incorporates some new techniques which are of some interest in their own right. We consider hadron operators both local in time, and nonlocal in time by one lattice spacing, finding that the latter give considerably better signals than the former. We test the dispersion relation by measuring correlators with nonzero momenta. To obtain realistic estimates of the statistical errors we employ the so-called "bootstrap" and "jackknife" methods.

There are a number of encouraging features in the results. First, the spectra for Wilson and staggered fermions agree, when compared in the appropriate way. Second, the flavor symmetry of the staggered fermions seems to be restored to within 5%. Finally, the best determined observables, f_π and m_ρ, give the same lattice scale to within 10%. The complete picture of the spectrum, however, is far from satisfactory, as we will discuss below.

II. THE ENSEMBLE

Our main ensemble of pure gauge fields consists of 36 configurations on an $18^3\times 42$ lattice. We use the single plaquette Wilson action with $\beta=6.2$. The configurations are generated using an optimized Metropolis multihit algorithm, with 20 hits per sweep, and 250 sweeps between analyzed configurations. Previous experiments with infrared-dominated observables (blocked loops) at $\beta=6.75$ convince us that these parameters are adequate to produce essentially independent gauge configurations. We will discuss this further below.

For SF's, our main data sample is obtained as follows. The first 10 lattices (2500 sweeps) after the cold start are discarded. On each of the next 36 configurations we calculated the quark propagators

$$G(n;n_0)=\langle \chi(n)\bar{\chi}(n_0)\rangle=\left\langle n\left|\frac{1}{\not{D}+m_q}\right|n_0\right\rangle , \qquad (1)$$

from two different base points separated by one timelike link. For the propagators from one base point (a_0) we use three values of quark mass: $m_q\in\{0.03,0.01,0.005\}$. For the base point one time step away (a_t) we use $m_q\in\{0.03,0.02,0.01\}$. In both cases we impose antiperiodic boundary conditions in all four directions, and solve the equations using a conjugate-gradient algorithm with an even-odd partition. We demand an accuracy on the propagators of

$$|r|^2=|(\not{D}^2-m^2)G+m\delta|_{\text{even}}{}^2\le 10^{-9}|G|_{\text{even}}{}^2 , \qquad (2)$$

where the norm only includes sites even relative to the base point, and δ is the δ-function source. This turns out to require on average about 300, 420, 720, and 1500 conjugate-gradient iterations for $m_q=0.03$, 0.02, 0.01, and 0.005, respectively. This accuracy is small enough that the statistical errors dominate the systematic errors point by point in the meson correlators. We verify this by running to an accuracy of 10^{-11} at $m_q=0.01$ and $m_q=0.005$ on 7 configurations. To check whether the sample we use for analysis is thermalized, we compute propagators from the base point a_0 on the 4th to 9th lattices of the 10 that we discard. There is some indication from the convergence time of the conjugate-gradient algorithm that these few configurations are not completely thermalized, but we find no discernible effect on the hadronic observables.

Because of the inherent expense we analyze fewer configurations with WF's. After discarding the first 3550 sweeps, we examine 23 configurations separated by either 250 or 500 sweeps. The quark propagators are calculated from a single source point per lattice, with periodic boundary conditions, using an accelerated Gauss-Seidel algorithm. As our convergence criterion we demand an accuracy of 10^{-7} in the pion propagator. We use four values of the hopping parameter: $\kappa\in\{0.30,0.31,0.32,0.325\}$. These require 300, 500, 700, and 900 iterations, respectively. To help speed the convergence of the algorithm we set the Wilson chiral-symmetry-breaking parameter to $r=\frac{1}{2}$. There is an additional, if small, motivation for this value from strong-coupling calculations: the ratio of nucleon mass to ρ mass is smaller at $r=\frac{1}{2}$ than at $r=1$.

III. STAGGERED FERMIONS

A. Operators

The simplest staggered fermion operators we consider are the usual local ones, generalized to include nonzero momentum. As is well known, these operators are not entirely satisfactory, in that they project out not one, but two different sets of quantum numbers with opposite parity. Omitting for brevity the terms because of the (anti)periodic boundary conditions in time, one parametrizes the local-local (LL) meson and baryon correlators as follows:

$$C_M^{\text{LL}}(t,\mathbf{p})=\left\langle \bar{\chi}\chi(0)\sum_{\mathbf{n}}\bar{\chi}\chi(t,\mathbf{n})\exp(i\mathbf{n}\cdot\mathbf{p})\phi_M(\mathbf{n})\right\rangle \sim C_+\exp(-m_+|t|)+C_-(-)^t\exp(-m_-|t|) , \qquad (3)$$

$$C_B^{\text{LL}}(t,\mathbf{p})=\left\langle \overline{\chi\chi\chi}(0)\sum_{\mathbf{n}\ \text{even}}\chi\chi\chi(t,\mathbf{n})\exp(i\mathbf{n}\cdot\mathbf{p})\right\rangle \sim C_+\exp(-m_+t)+C_-(-)^t\exp(-m_-t)\quad (t\ge 0)$$

$$\sim(-)^{t+1}C_+\exp(-m_+|t|)-C_-\exp(-m_-|t|)\quad (t<0) . \qquad (4)$$

Here we omit the obvious color contractions. The subscripts on the mass parameters indicate the contributions from pairs of states of opposite parity. The ϕ_m are the site-dependent phases which determine the spin and flavor content of the meson channels. These five different channels then contain $\pi/0^{+-}$, ρ/B, $\tilde{\rho}/A_1$, $\tilde{\pi}/\epsilon$, and N/Λ. The antiperiodic boundary conditions constrain the allowed momentum states $\mathbf{p}$: in the mesonic (baryonic) sector, each component p_i must be an even (odd) multiple of $\pi/18$. For the mesons we use $\mathbf{p}\in\{(0,0,0),(0,0,2),(0,2,2),(2,2,2),(0,0,4)\}$, while for the baryons we measure $\mathbf{p}\in\{(1,1,1),(1,1,3),(1,3,3),(1,1,5),(3,3,3)\}$. Using zero momentum, or any even momentum, for the baryon correlator would also yield a signal, but the allowed intermediate states would then include particles at all odd momenta. It is preferable to project separately onto the momentum eigenstates.

In each case we improve the signal by summing over the entire momentum orbit. That is, the factors $\exp(i\mathbf{p}\cdot n)$ above are replaced by $\cos(p_x n_x)\cos(p_y n_y)\cos(p_z n_z)$ plus permutations. Here we place the δ-function source at $\mathbf{n}=0$, and the antiperiodic boundaries between spatial coordinates 9 and -8. In the baryon correlator we only sum over the sublattice of sites where all spatial coordinates are even. Just as in the case of the zero-momentum baryon correlator with periodic boundary conditions,[10] the potential contributions from the rest of the sites cancel in pairs, once the average over gauge fields is performed. These are edge points, with one or more of their components equal to 9, which have no partners to cancel against; these would give a small contribution in $\mathbf{p}=0$ correlators, but have zero weight in channels modulated by cosines with odd momenta.

1. *Local-nonlocal in time (LNLT) meson and baryon correlators*

As we have described previously,[11,12] there is some advantage to using meson operators nonlocal in time (NLT). Like the local operators, NLT operators couple in general to two states (plus their excitations) with opposite parity. In the NLT case, however, the piece of the lattice operator responsible for creating one of the two parity partners corresponds in the continuum to an operator containing a derivative. The coupling to one state is therefore strongly suppressed relative to that of the other, and correlation functions involving the NLT operators are dominated by a single particle. In the correlator of the NLT operators with the usual local operators, the favored states turn out to be the pions and the ρ's, which we parametrize as

$$C_M^{\mathrm{NL}}(t,\mathbf{p})=\left\langle\bar{\chi}\chi(0)\sum_{\mathbf{n}}\bar{\chi}(t,\mathbf{n})U_4(t,\mathbf{n})\chi(t+1,\mathbf{n})\exp(i\mathbf{n}\cdot\mathbf{p})\phi_M(\mathbf{n})\right\rangle\sim C_+\exp(-m_+\,|\,t+\tfrac{1}{2}\,|\,)(-1)^t\quad(t\geq 0)$$

$$\sim C_+\exp(-m_+\,|\,t+\tfrac{1}{2}\,|\,)(-1)^{t+1}\quad(t<0)\,. \tag{5}$$

In Figs. 1(a) and 1(b) we plot the zero momentum LL and LNLT $\tilde{\rho}/A_1$ correlators for $m_q=0.01$. We note the almost complete absence of an A_1 contamination in the LNLT channel.

In a similar fashion, one can consider time split baryon operators. Here there are two sorts of operators—one with a single quark on the end of a link, the other with two quarks:

$$C_B^{\mathrm{NL1}}(t,\mathbf{p})=\left\langle\overline{\chi\chi\chi}(0)\sum_{\mathbf{n}}\chi(t,n)\chi(t,n)[U_4(t,n)\chi(t+1,n)]\exp(i\mathbf{n}\cdot\mathbf{p})\right\rangle\,, \tag{6}$$

$$C_B^{\mathrm{NL2}}(t,\mathbf{p})=\left\langle\overline{\chi\chi\chi}(0)\sum_{\mathbf{n}}\chi(t,n)[U_4(t,n)\chi(t+1,n)][U_4(t,n)\chi(t+1,n)]\exp(i\mathbf{n}\cdot\mathbf{p})\right\rangle\,. \tag{7}$$

Unlike in the meson case, there is no reason for the NLT baryon operators to couple predominantly to one state. Nevertheless we find some advantage over the local operators. In Figs. 2(a), 2(b), and 2(c) we show the data for the LL, LNL1, and LNL2 correlators for $m_q=0.01$ at the lowest accessible momentum, $\mathbf{p}=(\pi/18)(1,1,1)$. The improvement in the signal is not as dramatic as in the meson case, but using LNL1 does allow a slightly more stable extraction of the nucleon mass.

2. *Nonlocal-nonlocal in time (NLNLT) meson correlators*

Since we compute propagators from two different base points on each configuration, we are able to construct correlators with time-split operators on both ends as well. Whereas local meson operators have positive lattice charge-conjugation parity, these NLNLT correlators allow us to consider states in the negative lattice charge-conjugation sector as well. Thus, in addition to obtaining four channels dominated by the usual π, $\tilde{\pi}$, ρ, and $\tilde{\rho}$, we also get four channels containing new quantum numbers which are inaccessible with local operators.[13] These states are new flavors of the positive-parity particles, which we call $\tilde{\epsilon}$, $\tilde{A}_1$, and $\tilde{B}$. The fourth channel is the time component of the exactly conserved vector current, which does not excite any physical state:

$$C_M^{\mathrm{NN}}(t,\mathbf{p})=\left\langle\bar{\chi}_1(0,\mathbf{0})U_4\chi_2(1,\mathbf{0})\sum_{\mathbf{n}}[\bar{\chi}_2(t,\mathbf{n})U_4(t,\mathbf{n})\chi_1(t+1,\mathbf{n})\pm\bar{\chi}_1(t+1,\mathbf{n})U_4^{\dagger}(t,\mathbf{n})\chi_2(t,\mathbf{n})]\exp(i\mathbf{n}\cdot\mathbf{p})\phi_M(\mathbf{n})\right\rangle$$

$$\sim C_M\exp(-m_M\,|\,t\,|\,)(\pm)^t\,. \tag{8}$$

In these channels we allow for the possibility of two species of staggered fermions with different masses. We actually compute all possible correlators with quark masses $m_1 \in \{0.03, 0.01, 0.005\}$ at one base point and $m_2 \in \{0.03, 0.02, 0.01\}$ at the other, though only at $\mathbf{p}=0$. For comparison with the LL and LNLT correlators, in Fig. 3 we show the NLNLT ($\tilde{\rho}/B$) channel for $m_1 = m_2 = 0.01$. In Fig. 4 we show the negative lattice charge-conjugation ($\rho/\tilde{A}_1$) channel which is dominated by the $\tilde{A}_1$. We emphasize that rough as the correlator may be, using it is still better than trying to pick out the usual flavor of A_1 from underneath the ρ in the LL correlator of Fig. 1(a).

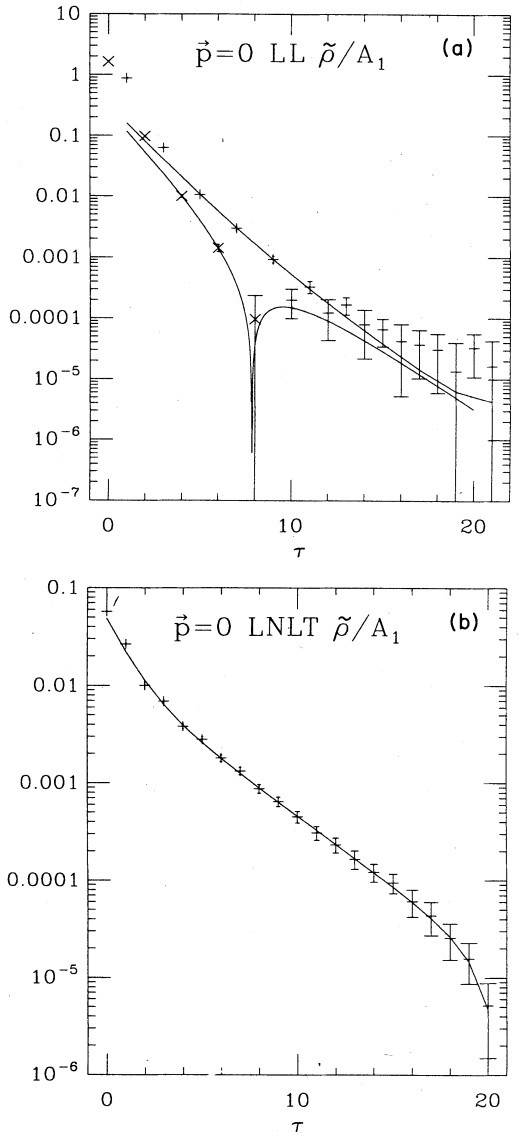

FIG. 1. (a) The zero momentum LL ($\tilde{\rho}/A_1$) correlator for SF with $m_q = 0.01$. The correlator has been symmetrized. To show the data on a log plot, points with negative sign are multiplied by -1 and represented by a $\times$, while positive points are represented by a $+$. The data show both a $\tilde{\rho}$ and A_1 signal at early times, but for $\tau > 10$ only the $\tilde{\rho}$ signal survives. The two curves are even and odd time pieces of a two-state fit. (b) The LNLT correlator for the same parameters as (a). The correlator has been antisymmetrized. The curve is a fit to the $\tilde{\rho}$ and a radially excited $\tilde{\rho}$. Note the dramatic decrease in the A_1 signal compared to (a).

Among the NLT operators are two rather special ones: namely, the charges of the $U(1)_V \times U(1)_A$ staggered-fermion symmetries. The vector current corresponding to quark number, $\bar{\chi}_n U_\mu \chi_{n+\mu} \eta_\mu(n) + \text{H.c.}$ (η_μ is the phase appearing in the staggered Dirac operator), is conserved when $m_1 = m_2$, and correlators of its charge should be time independent except for contact terms. In two-point functions the charge is acting on the vacuum, and one might expect the time-independent value to be zero. However, because we impose antiperiodic boundary conditions, there are contributions from quark paths which wrap around in the time direction. In addition to involving propagation along the entire time extent of the lattice, these are proportional to a spatial average of Polyakov lines. This quantity vanishes (in the confined phase) upon averaging over configurations, but is a small number on each configuration. All in all, the correlator should be constant for $t \neq 0$, with a very small, configuration-dependent value. We have found that checking this identity configuration by configuration provides a good control on the quality of the inverses for $m_q = 0.01$ and $m_q = 0.03$ (when we could set $m_1 = m_2$).

The current associated with the U(1) axial symmetry, $\bar{\chi}_n U_\mu \chi_{n+\mu} \eta_\mu(n) \epsilon(n) + \text{H.c.}$ [$\epsilon(n) = \pm 1$ on even/odd sites] is only partially conserved when $m_q \neq 0$, and any state with the quantum numbers of the pion is allowed to couple to it. As we go to the chiral limit, though, conservation of the current implies that $C_{\pi'}/C_\pi$ must vanish like m_π^2, where C_π is the coupling to the pion, and $C_{\pi'}$ is the coupling to any massive excited state. The correlator should therefore be more and more completely saturated with only the one-particle contribution. We confirm this expectation in Figs. 5(a) and 5(b), where we show the PCAC (partially conserved axial-vector current) channel for $m_1 = m_2 = 0.03$, and again for $m_1 = 0.005, m_2 = 0.01$. In each case the solid line is a single-particle fit, which tracks the data remarkably well even at small times.

Using the good currents allows us to calculate a detail of the hadron spectrum, the $\pi^+ - \pi^-$ mass difference.[14] Since quark mass differences do not contribute to lowest order, this difference is dominated by the electromagnetic contribution:

$$m_{\pi^+}{}^2 - m_{\pi^-}{}^2 = 2ce^2 f_\pi{}^2 , \tag{9}$$

where e is the electromagnetic charge and c is the coefficient of the term $e^2 f_\pi{}^2 \text{tr}(\Sigma Q \Sigma^\dagger Q)$ in the chiral Lagrangian. In terms of single flavor vector and axial-vector currents c is calculable as

$$c = \frac{1}{f_\pi{}^4} \int d^4x \langle V_\mu(0) V_\mu(x) - A_\mu(0) A_\nu(x) \rangle \Delta_{\mu\nu}(0,x) , \tag{10}$$

where $\Delta_{\mu\nu}$ is the photon propagator. This quantity vanishes as $m_q \to 0$ before one takes the infinite-volume lim-

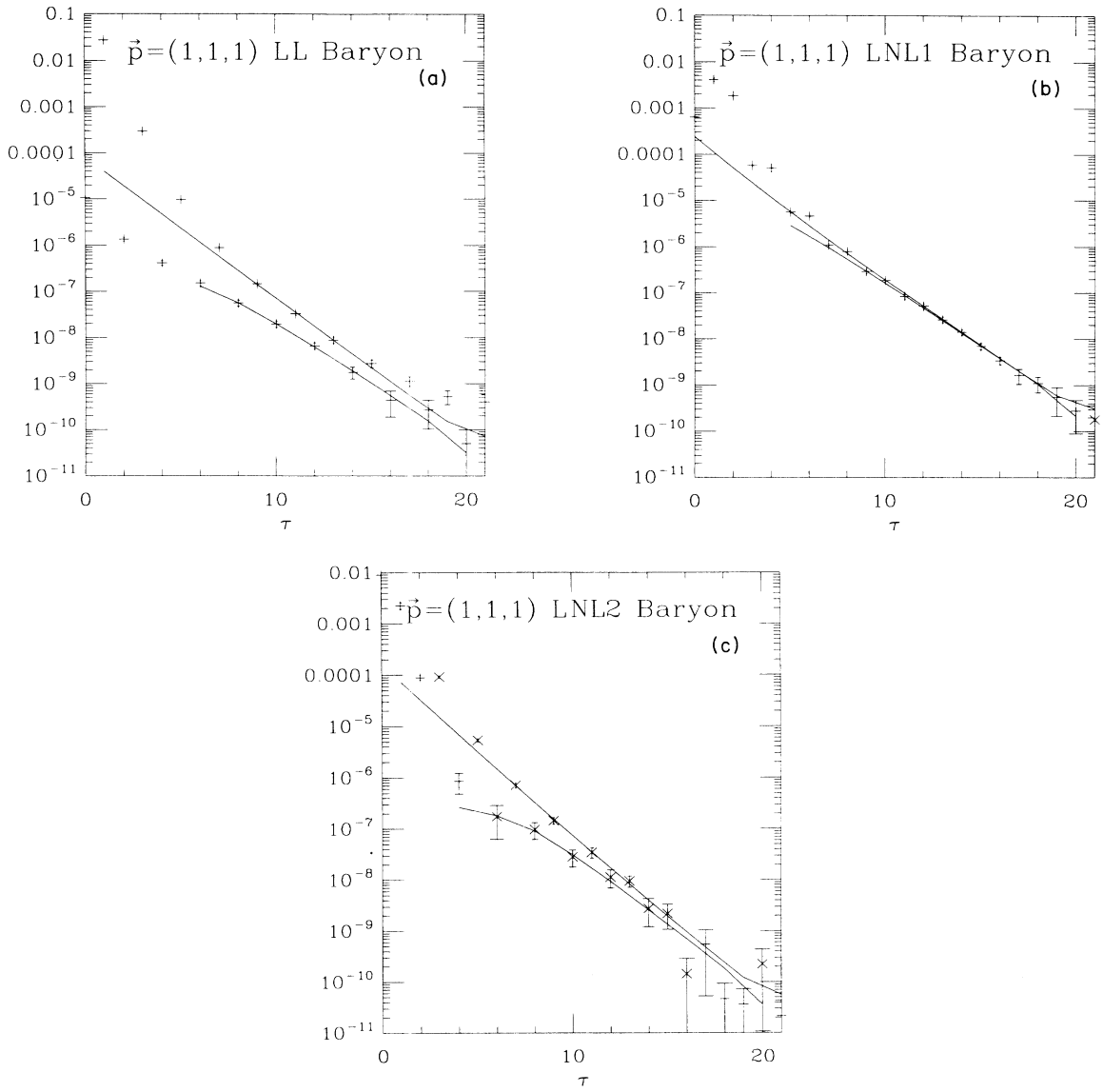

FIG. 2. The staggered baryon correlators for $m_q=0.01$. The momentum is the lowest allowed: $(\pi/18)(1,1,1)$. (a) LL. Note the clear Λ signal. The curves show a fit including N and Λ, with even and odd points connected separately. (b) LNL1. The Λ signal is much reduced. (c) LNL2. The Λ signal is slightly reduced relative to LL, but not by as much as LNL1. The signal is poorer than for LNL1.

it, and one must extract a number by extrapolation from finite quark mass just as one does for the chiral condensate. For the photon propagator we use an approximation to the infinite lattice Feynman gauge propagator defined by

$$\Delta_{\mu\nu}(x)=\delta_{\mu\nu}\frac{1}{V}\sum_p{}'\frac{e^{ip\cdot x}}{4\sum\sin^2(p_\mu/2)} . \tag{11}$$

The prime indicates that we replace the divergent $p=0$ mode (which is an artifact of the periodicity) by the finite constant

$$\int_{-\pi/N_s}^{\pi/N_s}\int_{-\pi/N_t}^{\pi/N_t}\frac{d^4p}{(2\pi)^4}\left[4\sum\sin^2(p_\mu/2)\right]^{-1} .$$

For the currents we use the appropriately scaled NLT operators. At $m_q=0.03$ we get the result $c=0.35\pm0.12$, while at $m_q=0.01$ we find $c=0.31\pm0.13$. This is to be compared to the strong-coupling result $c=1.06$ (Ref. 5) and to the physical answer $c=0.79$. We believe the discrepancy simply means that these quark masses are too large to be able to extrapolate this sensitive quantity to the chiral limit. Indeed if we separate out certain contributions to c which are known to vanish in the chiral limit, we find the result changes by 100%.

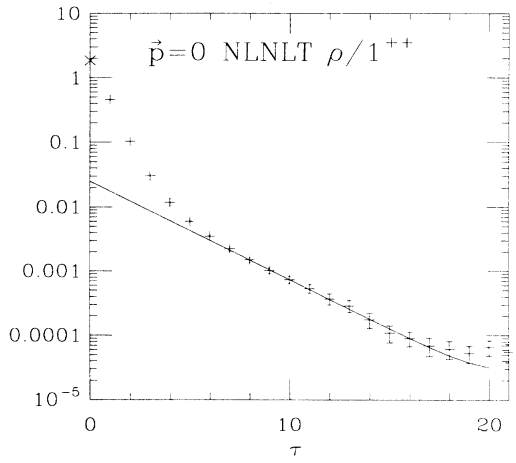

FIG. 3. The NLNLT SF positive lattice charge conjugation ($\rho/1^{++}$) correlator at zero momentum and $m_q=0.01$. The fit is a single particle ρ fit. Note the complete absence of 1^{++} signal.

B. Data analysis

To extract the mass of the lowest state in the correlators discussed above, we use a least-squares fit as follows. We begin by plotting each of the correlators and determining by eye the time slice τ_{max} where the signal disappears into noise. Then we fit to the appropriate sum of exponentials, including data points between some τ_{min} to τ_{max}, and look for a region of stability in the fit parameters as τ_{min} is varied. For channels with clean signals, the region begins typically around $\tau_{min}=8$. For the sake of uniformity, we take the fit parameters for $\tau_{min}=10$ as the definitive one whenever possible.

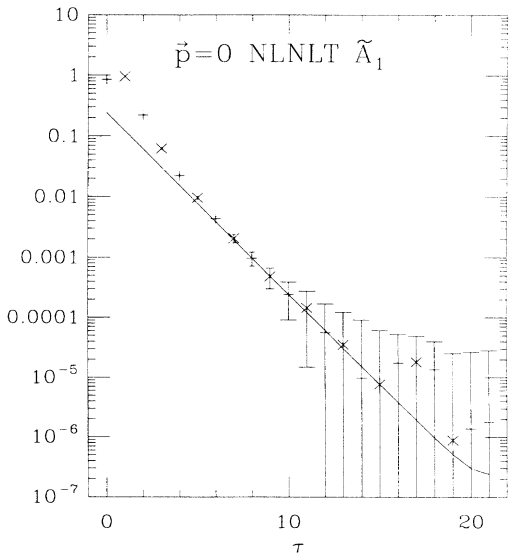

FIG. 4. The NLNLT SF *negative* lattice charge conjugation ($\rho/\tilde{A}_1$) correlator at zero momentum and $m_q=0.01$. The fit is to a single $\tilde{A}_1$.

The fitting function is in each case the sum of two exponentials. For the baryons and the LL mesons we fit to the two opposite parity partners, while in the LNLT and NLNLT meson channels we are allowed the luxury of fitting to a ground state plus an excited state. In the latter case the fit parameters of the heavy state are never stable enough to extract a mass, but including its contribution seems to increase the range of stability of the light mass.

To estimate the statistical errors of the fit parameters, we employ two powerful techniques: the "jackknife," as advocated, e.g., by Ref. 16, and its generalization called the "bootstrap" method.[17] The latter method is considered better in general, especially when dealing with

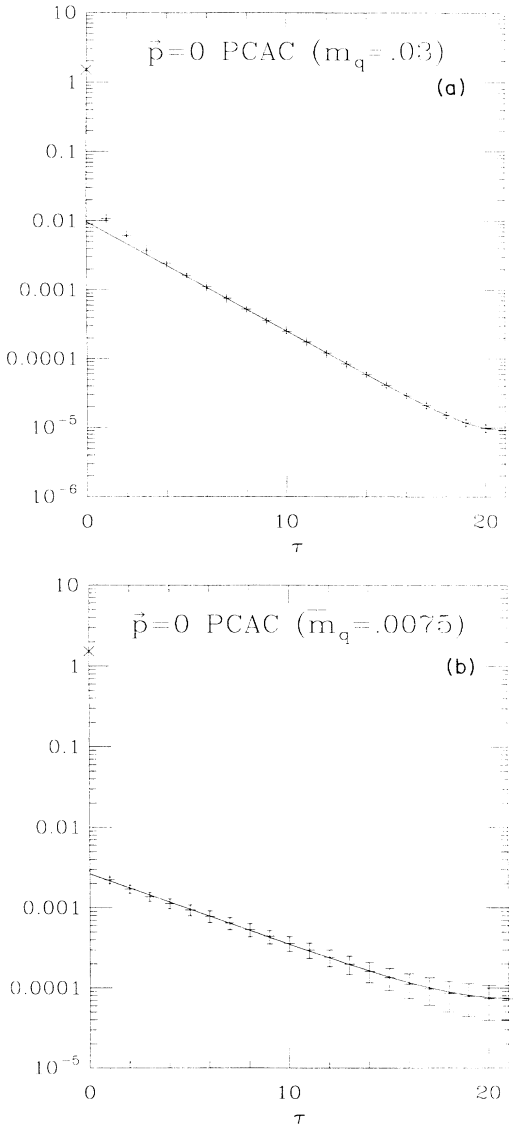

FIG. 5. The NLNLT SF positive charge conjugation ($\pi/0^{+-}$) correlator at zero momentum for (a) $m_q=0.03$ and (b) $\bar{m}_q=0.0075$. These are the correlators of the axial charge. The single particle fit works is good even at small τ.

small samples. The two should give convergent answers in the limit of large samples, and in practice for most observables they agree already with our sample size of 36 or more. Most of the errors we quote here are computed with the jackknife; those with asymmetric errors come from the bootstrap. We give a detailed discussion in the Appendix.

In any statistical calculation one needs to know how many truly independent configurations are included in the sample. Since the gauge configurations are taken from a single Markov chain, there are of course correlations from one configuration to the next. To control this effect we reanalyze the data after binning successive configurations in groups of two or more. The errors obtained from bin sizes of two or more all agree, and are perhaps 10% or 15% larger than those obtained without binning. From this we conclude that our configurations are essentially independent, at least as far as mesonic and baryonic observables are concerned. We also analyze the data involving local operators treating the correlators from the two different base points (a_0 and a_t) as if they are independent quantities. The errors so obtained for the pion mass are about a factor of $\sqrt{2}$ smaller than the true errors, and we take this is as evidence that the second base point adds essentially no independent statistical information. This is expected since the two base points are well within a correlation length of each other.

C. Chiral-symmetry breaking

The most simple fermionic quantity to measure is the condensate $\langle \bar{\chi}\chi \rangle$. This satisfies the usual Ward identity

$$\langle \bar{\chi}\chi \rangle = \mathrm{Tr} G(0;0) = m_q \sum_n |G(n;0)|^2 . \quad (12)$$

As we have pointed out before,[11] one also gets the derivative $(\partial/\partial m_q)\langle \bar{\chi}\chi \rangle$ directly with no extra work. We find it convenient to define the intercept

$$\mathrm{Int}(m_q) \equiv \left[1 - m_q \frac{\partial}{\partial m_q} \right] \langle \bar{\chi}\chi \rangle , \quad (13)$$

which we plot together with the condensate in Fig. 6. Considering the four lowest quark masses, we fit the condensate and its derivative to a cubic polynomial and determine the extrapolated value

$$\langle \bar{\chi}\chi \rangle |_{m_q=0} = 0.0105 \pm 0.0004 . \quad (14)$$

The next most simple quantity to measure is the pion mass, obtained from the exponential decay of

$$G_\pi(t) \equiv \left\langle \bar{\chi}\chi(0) \sum_{\mathbf{n}} \bar{\chi}\chi(t,\mathbf{n}) \phi_\pi(\mathbf{n}) \right\rangle \sim C_\pi \exp(-m_\pi t) . \quad (15)$$

In Fig. 7 we plot the square of the pion mass, as determined by fitting the correlator from time slice 10 and beyond. At the higher values $m_q = 0.01, 0.02, 0.03$, the pion mass shows very good Goldstone behavior—the extrapolated value at $m_q = 0$ is consistent with zero, within errors.[18] At $m_q = 0.005$, though, the pion mass lies above the linearly extrapolated value. This may be because of finite-size rounding, as for small enough m_q the pion mass is dominated by a contribution proportional to the inverse volume.[9] Alternatively, we may be seeing the first indication of chiral logarithms. Morel[19] has argued that these are to be expected in the quenched approximation, and he has found that the high-statistics SU(2) data of Ref. 20 are consistent with the expected form. Our data point can probably be made consistent with a similar form, but with only one errant point, we cannot provide a test. Excluding the lowest point, we make a linear fit and determine

$$\frac{m_\pi^2}{m_q} = 4.20 \pm 0.15 , \quad (16)$$

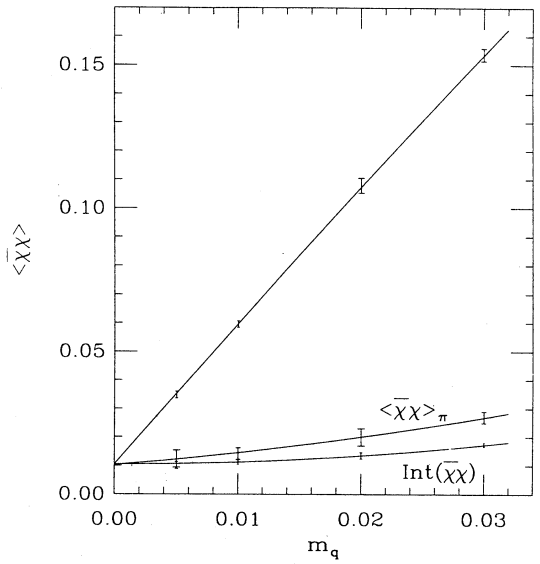

FIG. 6. The four-flavor value $\langle \bar{\chi}\chi \rangle(m_q)$ and its extrapolation to $m_q = 0$. $\langle \bar{\chi}\chi \rangle_\pi(m_q)$ and $\mathrm{Int}(m_q)$ are defined in the text.

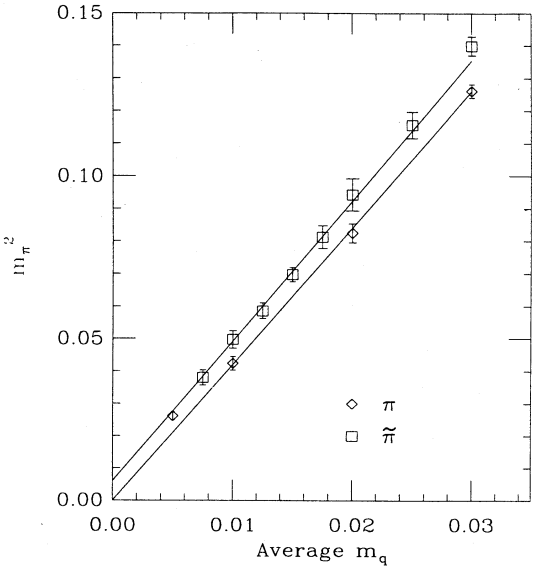

FIG. 7. The extrapolation of the SF m_π^2 and $m_{\tilde{\pi}}^2$ to $m_q = 0$. Only the LL values are used for m_π^2, and the fit is made without the point at $m_q = 0.005$.

which together with the result for $\langle\bar{\chi}\chi\rangle$ above yields a value for f_π:

$$f_\pi = \left[\frac{m_q}{m_\pi^2}\frac{\langle\bar{\chi}\chi\rangle}{2}\right]^{1/2} = 0.0354\pm0.001 \ . \tag{17}$$

The physical value $f_\pi = 93$ MeV then gives the scale of the lattice:

$$a^{-1}(f_\pi) \approx 2.6\pm0.1 \text{ GeV} \ . \tag{18}$$

This fixes the physical size of our spatial box at about 1.4 F. In physical units $m_q = 0.01$ gives a meson of mass of about 530 MeV, which fixes $m_q/m_s \approx 0.6$. The set of quark masses we use then corresponds to $m_q/m_s \in \{0.3, 0.6, 1.2, 1.8\}$.

One can also compute f_π from the amplitude C_π of the pion propagator for each quark mass and then extrapolate to physical quark masses. We express this determination by saturating the sum rule for $\langle\bar{\chi}\chi\rangle$ with the contribution of the pion intermediate state:

$$\langle\bar{\chi}\chi\rangle_\pi \equiv \sum_n \langle 0 \mid \bar{\chi}\chi(n) \mid \pi\rangle\langle\pi \mid \bar{\chi}\chi(n) \mid 0\rangle / \langle\pi \mid \pi\rangle = \frac{m_q C_\pi}{\tanh(m_\pi/2)} \ . \tag{19}$$

The errors on this quantity are larger, but as shown in Fig. 6, it extrapolates to the same value as $\langle\bar{\chi}\chi\rangle$, in agreement with the expectation that the pion dominates the channel as the quark mass decreases. Interpolating f_π to the point $m_q/m_s = 0.5$, we obtain the decay constant for a pseudoscalar with the mass of a kaon. We find $f_K/f_\pi = 1.20\pm0.06$.

D. Nonzero momentum

By measuring correlators with nonzero spatial momentum, we determine lattice dispersion relation $E(\mathbf{p})$ for a number of states. *A priori*, we do not know what the dispersion relation in a given channel is. We certainly expect something which reduces to the continuum formula for small $\mathbf{p}$, but the precise form of the order $|\mathbf{p}|^4$ lattice artifacts is some complicated function of the lattice action and the channel. In Fig. 8 we plot the results for the pion energy versus momentum for quark mass $m_q = 0.01$. For comparison we draw the curve appropriate to a free lattice boson with nearest-neighbor couplings:

$$4\sinh^2(E/2) = m_0^2 + \sum_i 4\sin^2(p_i/2) \ . \tag{20}$$

Fixing m_0, we find for the higher-momentum states what we consider reasonably good agreement with this dispersion relation. This is in spite of the sometimes poor quality of the signals at high momentum. Using the continuum dispersion relation gives an essentially indistinguishable plot. For the proton we can draw similar curves, but the errors on all but the lowest-momentum state are so large that no significant test can be made.

One can also determine f_π as a function of lattice momentum via the formulas

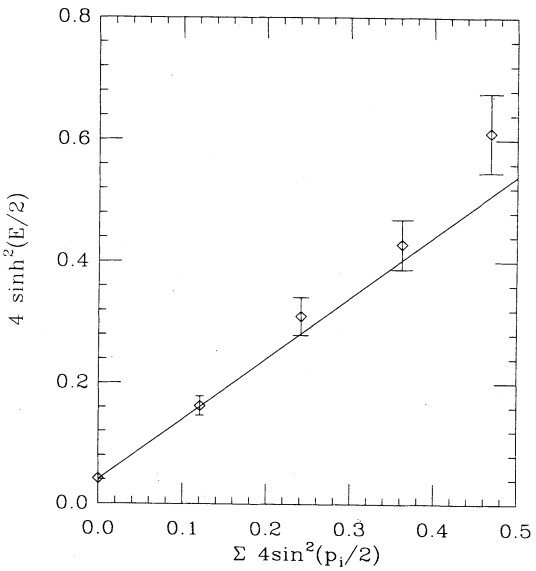

FIG. 8. The dispersion relation for the SF pion at $m_q = 0.01$. The line is the free meson dispersion relation given in the text, adjusted to agree with the zero spatial momentum data point.

$$\langle 0 \mid j_5^0 \mid \pi(\mathbf{p})\rangle \equiv E_\pi f_\pi^{\rm NL}(\mathbf{p}) \ ,$$
$$2m_q\langle 0 \mid \bar{\psi}\gamma_5\psi \mid \pi(\mathbf{p})\rangle \equiv (E_\pi^2 - \mathbf{p}^2) f_\pi^L(\mathbf{p}) \ . \tag{21}$$

Note that it is the Minkowski p^2 which appears on the right-hand side (RHS) of the latter equation. We extract $f_\pi^L(\mathbf{p})$ from the LL pion correlator, while from the LNLT correlator we get $[f_\pi^{\rm NL}(\mathbf{p}) f_\pi^L(\mathbf{p})]^{1/2}$. Table I gives the values we obtain using these equations. Lorentz symmetry would dictate that f_π should be momentum independent, and our results are consistent with this. We could instead demand the continuum dispersion relation and insert m^2 in place of $E_\pi^2 - \mathbf{p}^2$ in the second equation. In that case we find some momentum dependence in f_π, though the values at the lowest momenta still agree within errors.

E. The spectrum

The results for the hadron spectrum at zero momentum are given in Tables II–IV. For the mesons the masses are extracted from the NLNLT correlators, except in those cases noted in the tables. For the proton the cleanest signal comes from the LNL1 channel, while for the Λ the most reliable estimate is in the ordinary LL channel. For both baryons we extrapolate from the $\mathbf{p} = (\pi/18)(1,1,1)$ state to the state at rest using the continuum dispersion relation, though any reasonable lattice dispersion relation would give answers indistinguishably close. In all cases the quoted masses are consistent with those determined from other channels, though there are some systematic biases. The clearest bias is that the pion mass comes out somewhat higher in the NLNLT channel than in the LL channel (as shown in Fig. 9).

As discussed above and shown in Fig. 7, the π exhibits the expected Goldstone behavior. A pleasing result is

TABLE I. Values obtained using Eqs. (20) and (21) in text.

p	$m_q = 0.01$ pion E_π(LL)	E_π(LNL)	f_π^L	$(f_\pi^L f_\pi^{NL})^{1/2}$
(000)	0.208(5)	0.203(6)	0.043(3)	0.042(2)
(002)	0.40(3)	0.39(2)	0.047(9)	0.043(3)
(022)	0.59^{+15}_{-08}	0.55(3)	0.039(30)	0.043(5)
(222)	a	0.64(3)	a	0.048(7)
(004)	a	0.76(4)	a	0.040(15)

[a]Signal too poor to fit.

that the $\tilde{\pi}$ stays fairly degenerate with the π at the lighter quark masses, and seems to approximate Goldstone behavior as well. As shown in Fig. 7, the $\tilde{\pi}$ mass does not extrapolate precisely to zero, but is clearly anomalously light compared to the other states. Likewise the ρ and $\tilde{\rho}$ seem fairly degenerate except at lowest quark mass, where the signal is rather hard to fit and the statistical errors become large. We take this as evidence that the SU(4)-flavor symmetry is being dynamically restored.

In Fig. 9 we plot $m_\pi{}^2$, $m_\rho m_{\tilde{\rho}}$, m_N, and m_Λ as a function of quark mass. The linear extrapolation looks reasonable for all channels. In each channel we fit the particle mass and its square to the form $Am_q + B$ and extrapolate to $m_q = 0$. These extrapolated values are also compiled in Table II. The two different extrapolations are meant to give some indication of $O(m_q{}^2)$ corrections, though we use the linear extrapolation for fixing the scale. We note that the two flavors of ρ meson extrapolate together to $m_\rho a = 0.31 \pm 0.03$, so we get $a^{-1}(m_\rho) = 2.5 \pm 0.3$ GeV, which is consistent with $a^{-1}(f_\pi)$. We get an independent estimate of the lattice scale from the slope of the fits, i.e.,

$$a^{-1} = \frac{m_K{}^2 - m_\pi{}^2}{m_{K^*} - m_\rho} \left[\frac{A_\rho}{A_\pi} \right] = 2.0 \pm 0.5 \text{ GeV} .$$

Finally, if we use the nucleon mass to set the scale we find $a^{-1}(m_N) = 2.05 \pm 0.2$ GeV.

The most disturbing feature of the spectrum is the consistently large value for the nucleon mass. The ratio m_N/m_ρ starts out close to the heavy-quark value of $\frac{3}{2}$, and never comes down as we decrease the quark mass.

Also perturbing are the results for the $\tilde{\epsilon}$. At large quark mass, one has $m_{\tilde{A}_1} \approx m_{\tilde{\epsilon}} > m_\rho$. But for $m_q < 0.02$ we find $m_{\tilde{\epsilon}} \approx m_{\tilde{\pi}}$. In other words, for small quark mass the $\tilde{\epsilon}$ is showing Goldstone behavior. Although the errors are quite large, they are barely large enough to raise $m_{\tilde{\epsilon}}$ to the level of m_ρ. We can think of at least two explanations. The first is that there is mixing with a pion with different quantum numbers. There are indeed pions with negative lattice charge conjugation, and with the same ξ_4 parity[12] as the $\tilde{\epsilon}$, so the signal we see could be from such a state. However, the mixing is forbidden by the lattice translation symmetries, and so could only occur because we have a finite sample of configurations. The second possibility is that our result is real, but that $m_{\tilde{\epsilon}} a$ stabilizes at around 0.2, which corresponds to physical mass of about 0.5 GeV. Only further work will distinguish these options. To our knowledge, no other groups have looked at states with negative lattice charge conjugation.

The remaining positive-parity states are less controversial. Where we have measurements of both, the A_1 and $\tilde{A}_1$ are consistent with each other. The $\tilde{B}$ tends to be slightly lighter than the $\tilde{A}_1$, but both are considerably heavier than the ρ, and, at the smallest m_q, are also heavier than the nucleon. These are the expected orderings.

IV. WILSON FERMIONS

For WF's the fitting necessary is more straightforward. Only states of one parity contribute to each

TABLE II. Staggered meson spectrum: odd parity.

Mass	π	$\tilde{\pi}$	ρ	$\tilde{\rho}$
0.03	0.355(03)[a]	0.374(4)	0.45(1)	0.47(1)
0.025	0.333(10)	0.340(4)	0.43(2)	0.45(2)
0.02	0.287(05)[a]	0.307(4)	0.40(2)	0.43(2)
0.0175	0.310(40)	0.285(6)	0.41(4)	0.41(4)
0.015	0.274(23)	0.264(7)	0.38(3)	0.39(3)
0.0125	0.270(40)	0.242(7)	0.38(5)	0.39(5)
0.01	0.206(05)[a]	0.223(7)	0.35(4)	0.36(5)
0.0075	0.213(33)	0.195(9)	0.35(7)	0.36(7)
0.005	0.153(09)[a]	0.120(50)[a]	0.44^{+21}_{-11}[a]	0.34^{+14}_{-07}[a]
0(lin)	0.18(2)	0.149(6)	0.31(3)	0.32(3)
0.(sq)	−0.02(3)	0.057(26)	0.30(4)	0.31(4)

[a]LNLT correlator.

TABLE III. Staggered meson spectrum: even parity.

Mass	ϵ	$\tilde{\epsilon}$	A_1	$\tilde{A}_1$	$\tilde{B}$
0.03	0.56(3)[a]	0.64(09)	0.63(13)[a]	68(11)	0.55(13)
0.025		0.56(13)		0.68(10)	0.62(13)
0.02	0.44(5)[a]	0.46(9)		0.69(13)	0.65(6)
0.0175		0.31(6)		0.67(10)	0.57(9)
0.015		0.30(9)		0.70(10)	0.57(10)
0.0125		0.25(5)		0.66(12)	0.51(11)
0.01	0.31(10)[a]	0.24(9)	0.66(61)	0.70(10)	0.52(13)
0.0075		0.20(7)		0.64(17)	0.42(16)
0.005					

[a]LL correlator.

meson correlator, though each state propagates in both directions. In the baryon channels we include forward propagation of the nucleon and δ, and backward propagation of opposite-parity baryons. The fits to determine the masses are made for $\tau \geq \tau_{\min}$. Stable masses and amplitudes are found for $\tau_{\min} \geq 11$. Fixing these parameters, we then attempt to include a radial excitation: though the fits are good, the mass of the radial excitation is not stable. As a check, we fix the radial mass and amplitude to those determined at some τ, and redetermine the lowest-state parameters for $\tau_{\min} \geq 11$. We also make independent unconstrained two state fits. All these fits yield essentially identical results for the lowest state.

The results for WF's are collected in Table V. The masses given are those determined with $\tau_{\min}=12$. We calculate the statistical errors by taking various subsets of 10 configurations and determining the masses for these. The problems with this straightforward method are discussed in the Appendix. We estimate the systematic errors by the size of the change in mass between $\tau_{\min}=9$ and 12. The systematic errors are larger, and we quote these in the table. That the systematic errors dominate is no surprise as we are using fairly heavy quarks. Another possible source of systematic error is the existence of exceptional configurations on which masses differ considerably from those on the bulk of the configurations.[21] We find that none of our configurations is exceptional.

On our large lattice we see quite clearly the asymptotic single-particle exponential. To show this, we plot in Fig. 10 the effective mass $m_{\rm eff}$ for π, ρ, N, and Δ at our largest value of κ (smallest quark mass). For the mesons the effective mass is found by solving

$$\frac{\Gamma(\tau+1)}{\Gamma(\tau)} = \frac{e^{-m_{\rm eff}(\tau+1)} + e^{-m_{\rm eff}(42-\tau-1)}}{e^{-m_{\rm eff}\tau} + e^{-m_{\rm eff}(42-\tau)}}, \tag{22}$$

while for the baryons we use $m_{\rm eff}=\ln[\Gamma(\tau)/\Gamma(\tau+1)]$ and avoid the opposite-parity state propagating backwards by a cutoff at $\tau=16$. It is only for $\tau \geq 11$ that the correlation function is dominated by a single mass. We find that this value of $\tau_{\min}$ is independent of κ.

Excluding the smallest value of κ (heaviest quark mass), we extrapolate $m_\pi{}^2$ to zero and find the critical value $\kappa_c=0.3327\pm0.0008$. We show in Table V the extrapolated results for a fit of the particle masses and their squares to the form $A\kappa^{-1}+B$. Also tabulated is the Wilson quark mass parameter $m_q^W=\ln[1+\frac{1}{2}(\kappa^{-1}-\kappa_c{}^{-1})]$. In Fig. 11 we show the linear extrapolation. From the masses of the ρ, N, and Δ, we determine the lattice scale to be $a^{-1}(m_\rho)=2.5\pm0.2$ GeV, $a^{-1}(N)=1.9\pm0.1$ GeV, and $a^{-1}(\Delta)=2.1\pm0.1$, respectively. The first two are in agreement with the corresponding scales found with SF's: once again the nucleon

TABLE IV. Staggered baryon spectrum.

Mass	$N(\mathbf{p})$	$N(\mathbf{p}=0)$	$\Lambda(\mathbf{p})$	$\Lambda(\mathbf{p}=0)$
0.03	0.79(2)	0.73(2)	0.89(4)	0.83(4)
0.02	0.73(2)	0.67(2)	0.77^{+9}_{-7}	71^{+9}_{-7}
0.01	0.64(3)	0.59(3)	0.73(5)	0.67(5)
0.005	0.60(4)	0.52(4)	0.72^{+8}_{-5}	66^{+8}_{-5}
0(lin)		0.48(3)		0.60(6)
0(sq)		0.46(4)		0.59(7)

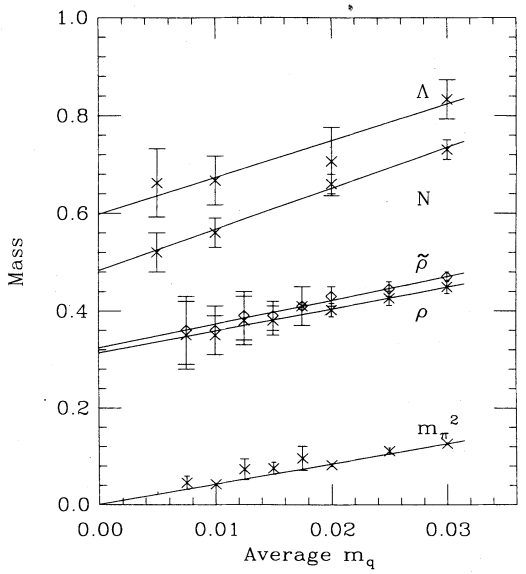

FIG. 9. Linear extrapolations of various SF masses to $m_q=0$. The resulting values are given in Tables II and IV.

TABLE V. Wilson hadron spectrum.

κ	m_q	π	ρ	A_1	δ	N	Δ
0.30	0.152	0.643(1)	0.675(5)	0.82(1)	0.82(1)	1.07(1)	1.09(1)
0.31	0.105	0.507(5)	0.553(5)	0.68(1)	0.70(2)	0.90(1)	0.93(1)
0.32	0.058	0.37(1)	0.443(6)	0.55(1)	0.64(5)	0.715(8)	0.76(1)
0.325	0.035	0.29(1)	0.391(10)	0.45(2)		0.62(1)	0.70(1)
lin	0	0.19(1)	0.313(11)	0.37(2)	0.57(11)	0.49(1)	0.58(2)
sq	0	0	0.272(17)	0.31(4)	0.58(13)	0.42(2)	0.55(2)

has come out too heavy relative to the ρ. Lastly, from the slopes of the fits to $m_\pi{}^2$ and m_ρ we get $a^{-1}=2.1\pm0.2$ GeV. This is also in agreement with the analogous quantity for staggered fermions, and squarely sided with the baryons in the debate over the scale.

V. LANDAU-GAUGE GLUON PROPAGATOR

On our ensemble of 36 configurations we have also calculated the gluon propagator after changing each lattice to Landau gauge.[22] The gluon propagator is not a physical quantity since it is not gauge invariant. Nevertheless, it is of importance for phenomenological models of QCD. Studying it may provide some insight into the transition between the short-distance asymptotically free behavior and the long-distance nonperturbative physics. We expect that the gluon will carry a screening charge cloud along with it, and effectively appear as a massive particle. This is what we look for in our correlators.

The Landau gauge fixing condition, $\partial_\mu A_\mu=0$, can be interpreted as the solution to the variational problem of minimizing $\int d^4x\ \mathrm{tr}(A_\mu A_\mu)$. We implement the lattice version of the Landau gauge condition by maximizing

$$\sum_{x,\mu} \mathrm{Re\,Tr} U_\mu(x)\ . \tag{23}$$

In the continuum, there exists the well-known problem of Gribov ambiguities for Landau gauge. That is to say, the differential constraint is unable to fix the gauge completely, there being more than one solution to the gauge condition on certain configurations. The changeover to the global integral condition is likely to get rid of this problem in principle, but in practice finding the global maximum without getting trapped in local ones depends very much on the searching algorithm. We partition the lattice into even and odd points, and then alternating between them gauge transform the lattice so as to maximize the quantity in the equation above. This process appears to converge well, though not guaranteed to do so. We monitor the average value of $1-\mathrm{Re\,Tr}V(x)$, where $V(x)$ is the gauge transformation matrix at site x, and stop the iterative process when this value falls below 10^{-6}. This typically required around 800–1000 iterations. The stability of the answer was checked by running to the accuracy of 10^{-7} on some configurations and looking at the changes in the gluon propagator.

We choose to define the gluon field as $A_\mu(x)=[U_\mu(x)-U_\mu^\dagger(x)]/2i$. The results for the zero-momentum correlation functions $\langle \mathrm{tr}[A_\mu(0)A_\mu(t)]\rangle$ are displayed in Fig. 12. As a consequence of the gauge-fixing condition and the periodic boundary conditions, the A_0 correlator is expected to be time independent.

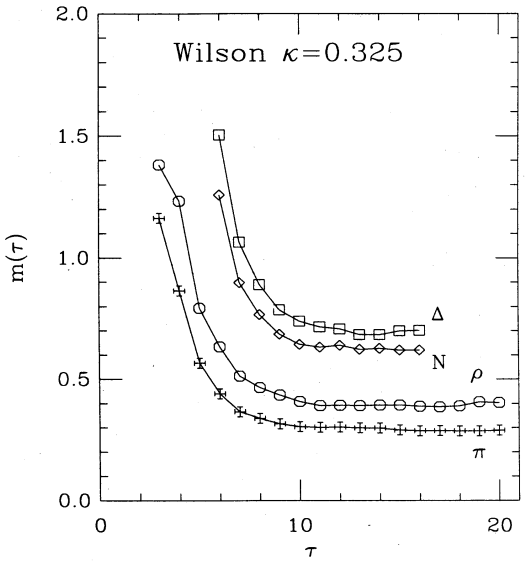

FIG. 10. The effective mass for Wilson fermions as a function of τ. The data are for $\kappa=0.325$. m_{eff} is defined in the text. The statistical errors are smaller than the symbols.

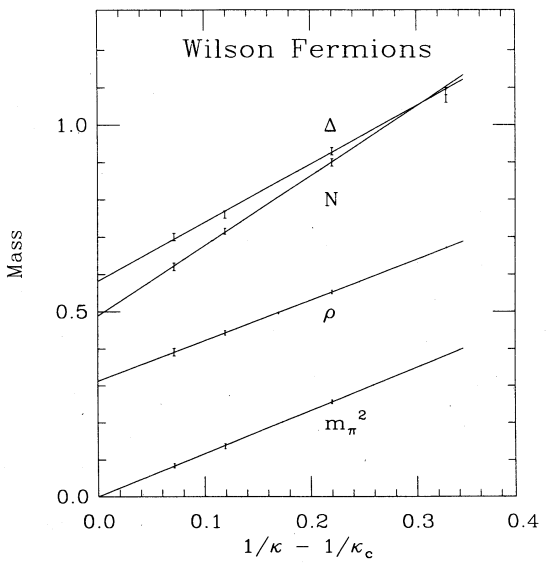

FIG. 11. Linear extrapolations of the WF mass results to κ_c. The resulting values are reported in Table V.

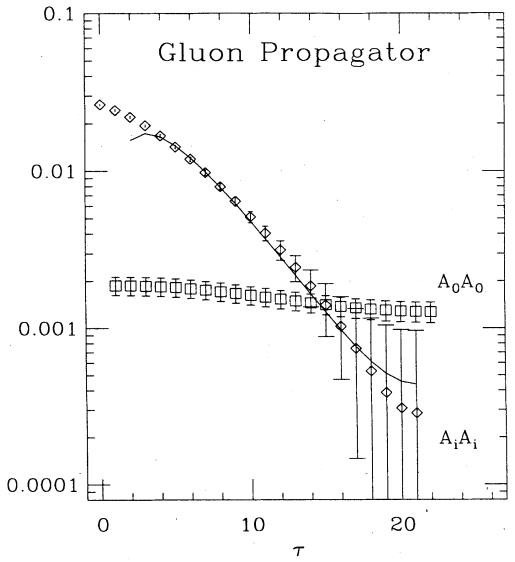

FIG. 12. The zero-momentum gluon propagator in the Landau gauge. The fit to the space-space correlator includes one gluon and one ghost.

Its observed variation actually provides a good check on the convergence of our iterative algorithm. The interesting correlator is $\langle \mathrm{tr}[A_i(0)A_i(t)]\rangle$. We note that at short distances it is quite flat, as is to be expected from an asymptotically free theory. Also the correlator cannot be fit by a sum of contributions from positive-definite states only. Instead it is well fit by a two exponential form containing a gluon of mass 0.241 ± 0.034 and a ghost of mass 0.501 ± 0.031. Using the scale determined by the hadron spectrum, this corresponds to a screened gluon weighting about 600 ± 90 MeV, and a screened ghost at about 1250 ± 80 MeV. Though one cannot define a truly massless state on a periodic lattice, the clarity of the data and the magnitude of the mass make it unlikely that we are observing a finite-volume or some other spurious effect.

VI. DISCUSSION

There are a number of pleasing features in these results. The chief among them is the consistency between the Wilson and the staggered spectra. The extrapolated values at $m_q=0$ agree, but, more importantly, the results at finite quark masses also match. The Wilson states for $\kappa=0.32$ ($m_q^W=0.058$) match very closely the staggered states at $m_q=0.03$, while $\kappa=0.325$ ($m_q^W=0.035$) corresponds to something slightly less than staggered $m_q=0.02$ A similar ratio of m_q^W to m_q^S was also observed by Hamber[23] at $\beta=6.0$. Comparing the data for SF's with WF's at corresponding points, we do find that the signal is significantly cleaner for WF's.

It is also gratifying that the staggered flavor symmetry seems to be restored at the level of $\approx5\%$. This is an improvement over the results at $\beta=6$ (Ref. 24). Together with the closeness of the spectra of SF's and WF's this indicates that $\beta=6.2$ the lattice spacing may be fine enough that the details of the fermion action have ceased to be relevant. We cannot say whether $\beta=6.2$ is in the asymptotic scaling regime, but we note that the region from $\beta=6.0$ to $\beta=6.2$ is not. If the perturbative two-loop scaling formula is applicable, we get $a^{-1}(\beta=6.0)\approx0.8a^{-1}(\beta=6.2)$. Previous calculations[23–25] using m_ρ to set the scale, give $a^{-1}(\beta=6.0)$ in the range 1.6–1.9 GeV. Thus the scale is changing faster than predicted by asymptotic scaling, a result consistent with the well-known dip in the β function determined from several other physical quantities.

The situation with the baryons is nicely summarized in the so-called Edinburgh plot displayed in Fig. 13. This plots m_N/m_ρ as a function of m_π/m_ρ for each of our data points. No data point is shown for SF's at $m_q=0.005$, since we have no reliable estimate for the ρ mass there. For comparison we also show the curve one gets from the naive quark model including hyperfine splittings.[26] Again, the agreement between staggered and Wilson fermions is apparent in that the points for both form a single curve. The disagreement with the physical value of m_N/m_ρ is also evident. None of the measured points lie under the line $m_N/m_\rho=1.5$.

It is worthwhile comparing the masses we have been using to the physical strange-quark mass. To do this we find the lattice quark mass which yields a pseudoscalar with physical mass ≈0.69 GeV. This is the value given by current algebra for an $\bar{s}s$ meson in the absence of pure gluonic intermediate states. Using the scale $a^{-1}=2.5$ GeV, we find that $m_s a\approx0.016$ for SF's and $K_s\approx0.326$ for WF's. Thus for SF's our lightest-quark mass is about $m_s/3$, though our lowest mass with a reliable determination of m_π, m_ρ, and m_N is about $2m_s/3$. These lowest masses are comparable to those used by others with SF's at $\beta=6$ (Refs. 24 and 25). For WF's, our lightest mass is just above m_s, in common with all

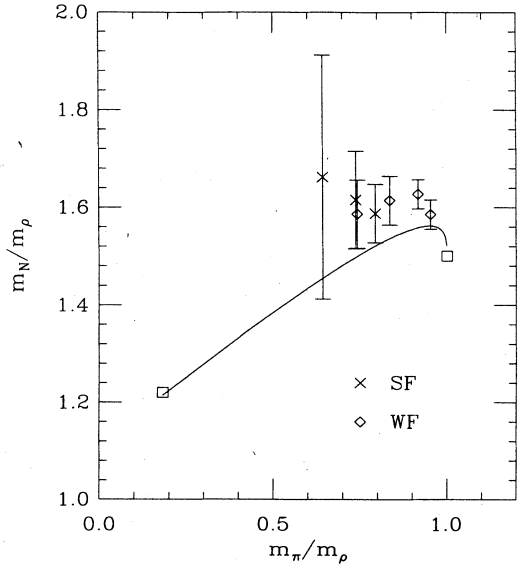

FIG. 13. Edinburgh plot of both SF and WF data. The SF point at $m_q=0.005$ is not included because of the very large errors in m_ρ. The squares are the known limiting points, and the curve is a naive quark model.

other large-scale calculations.[23,27]

What are we to make of the apparent problem with the baryons? One can consider several explanations. (1) It may be that we are not in the scaling regime, even at $\beta=6.2$. The ratio of nucleon to ρ mass may simply decrease towards the correct value as β increases. In view of the agreement between staggered and Wilson fermions, and of the restoration of staggered flavor symmetry, we think this is an unlikely explanation for the large effect. (2) The results are affected by the finite size of the small box. This is a more reasonable explanation, particularly at the lightest-quark masses, for which the nucleon states are largest. Certainly a *physical* proton would have to be squashed into our small box (or rather, crushed against its neighbors). This would raise the mass which we measure. Indeed at the lightest staggered quark mass ($m_q=0.005$) we may be seeing finite-size effects in m_π. We expect the (larger) baryons to feel the finite size more strongly than the meson states. (3) The extrapolations are from quark masses that are too heavy. This is certainly true to some extent. It does not, however, explain why our data points lie systematically above the curve in Fig. 13. (4) Finally, to be honest we should consider the possibility that both the points and their extrapolation are correct, and that we are simply seeing a defect of the quenched approximation. Indeed there is good reason to be suspicious of the quenched approximation. Given the present experimental value of the so-called nucleon σ term, chiral perturbation theory leads one to the surprising conclusion that one-third of the nucleon mass is due because of *dynamical* strange quarks. The analysis is by no means uncontroversial,[28] but if correct it would affect most every other quenched observable as well.

Comparing our results with earlier work at $\beta=6$ (Refs. 23–25) (or work using an improved action with a similar scale[27]), it appears that going to smaller lattice spacing has not improved the agreement with the continuum spectrum. It is instructive to divide the data into two regions: (1) $m_q > m_s$ and (2) $m_q < m_s$. Region (1) contains all the WF data and most of the SF data. In the Edingburgh plot this region has $m_\pi/m_\rho \geq 0.67$, using the $\bar{s}s$ mass of 0.69 GeV, and $m_\phi=1.02$ GeV. In fact, a more careful calculation, using the relativistic quark model of Capstick, Godfrey, and Isgur,[29] finds that for $m_q=m_s$ one should expect $m_\pi/m_\rho=0.75$ and $m_N/m_\rho=1.45-1.48$ (Ref. 30). This calculation is likely to be quite reliable for such relatively heavy quarks, and it is a considerable challenge to the lattice to surpass it. Refs. 23, 25, and 27 indeed find mass ratios close to these values for $m_q \approx m_s$, while[24] finds m_N/m_ρ slightly too high. Our data are also too high, similar to those of Ref. 24.

It is extremely difficult to convincingly extrapolate from data in region (1) to $m_q=0$. It is in region (2) that the quarks become truly light, and m_N/m_ρ makes its major departure from $\frac{3}{2}$. Thus it is crucial to measure masses in this region. With SF's, Refs. 24 and 25 have one (maybe two) such points. Though they disagree somewhat on m_N, it is clear that they both find m_N/m_ρ to be too high. We have a considerable number of points for m_ρ in region (2), though only at two do we have m_N, and only at one of these can we quote a reliable value for m_N/m_ρ. This single point gives an even larger m_N/m_ρ than the heavier quarks of region (1). Thus, one again, moving to larger β has not improved matters.

Clearly a resolution of the problem with baryons requires study on a larger lattice at the same β, with emphasis on extracting π, ρ, and N masses for $m_q < m_s$. This might also shed further light on the problem of the anomalously light $\tilde{\epsilon}$. We hope that the next generation of dedicated machines will be able to penetrate to this crucial region of parameter space.

ACKNOWLEDGMENTS

We thank the C Division of the Los Alamos National Laboratory for supplying us with time on Cray X-MPs. We also thank Nathan Isgur for useful correspondence. A.P., G.K., and S.S. thank Los Alamos for its support while part of this work was completed. The work of G.G. and S.S. was supported in part by DOE Contracts Nos. DE-AC02-76-ER03130.A0B (Task D) and DE-AC03-76SF00515, respectively. G.K. acknowledges the support of NSF Contract No. PHY82-15249. R.G. would like to thank the J. Robert Oppenheimer Foundation for financial support.

APPENDIX: STATISTICAL ERRORS

Given a set of N relatively independent propagators G.G. and S.S. was supported in part by DOE Contracts Nos. DE-AC02-76-ER03130.A0B (Task D) and DE-AC03-76SF00515, respectively. G.K. acknowledges the support of NSF Contract No. PHY82-15249. R.G. would like to thank the J. Robert Oppenheimer Founda-

$$\chi^2(\alpha)=\sum_t \frac{[\bar{G}(t)-C(t;\alpha)]^2}{\sigma(t)^2} \ . \tag{A1}$$

Here $\bar{G}(t)$ and $\sigma(t)$ are the mean and deviation on each time slice, and $C(t;\alpha)$ is the function to be fit by varying the parameters α. The errors ascribed to the best fit values are then conventionally defined by the variation $\delta\alpha$ in a given parameter needed to increase the χ^2 by one unit. When the fluctuations from one time slice to the next are correlated this estimator is seriously flawed. To take an extreme example, suppose that the individual correlators $G_i(t)$ were each of the form $A_i \exp(-Mt)$, with a common exponential fall off. Then after averaging and fitting, the standard method would indeed give the correct central value M, but could give a considerable δM. Clearly we need a method which would show no variation in M.

One reasonable method is "cross validation," which is almost universally employed in simulations to date. One divides the data into subensembles containing several configurations each. In each subensemble separately one computes the masses by fitting the average as above, and takes the dispersion in the fit values as an estimate of the statistical errors. There are at least two objections to this method. A practical drawback is simply the size of the samples required—each subensemble must contain enough configurations to show a reasonable signal, and

then one needs several of these subensembles to make an estimate of the dispersion. In our case, one needs subensembles of 10 or more configurations in some channels to see a signal worthy of being fit, which would then give only three or four points whose scatter is to give the error. Another problem is that these three or four points are drawn from an unknown distribution, and the conventional relationship between the error of the mean and the width of the distribution may not hold. Only in the limit of very large subensembles should we expect the fluctuations in the fit parameters to become Gaussian.

The first problem is cured in the so-called jackknife method, named for its versatility and all around usefulness. As described, e.g., in Ref. 16, this method proceeds by considering the N subensembles of $N-1$ configurations obtained from the original sample by removing a single configuration. One then fits to the average of each subensemble, and obtains a distribution of N values for each fit parameter. In Fig. 14(a) we show the jackknife distribution for the $\tilde{\rho}$ mass at $m_q=0.005$. The jackknife estimate of the errors is given by a suitable rescaling of the variance in the fit parameters:

$$\delta\alpha=[N(\langle\alpha^2\rangle-\langle\alpha\rangle^2)]^{1/2}\ . \qquad \text{(A2)}$$

The advantage over cross validation comes in that one can get stable results for the central value even with relatively small samples. However, the jackknife distribution need not be Gaussian, as is evident in Fig. 14(a). One could use the histogram to extract asymmetric errors, but with such a small population the results for the errors may be unstable.

The bootstrap method[17] is a generalization and improvement of the jackknife. It requires somewhat more work, but is known to be a more robust method than the jackknife. In fact the jackknife is an approximation to the bootstrap. Starting from the original N configurations, one considers the huge set of all possible sets of N configurations obtained by drawing from the original set *with* replacement. That is, these bootstrap samples can contain a given configuration once, several times, or not at all. On average, a fraction $1-[(N-1)/N]^N \approx(e-1)/e\approx\frac{2}{3}$ of the N configurations will be represented in a given bootstrap sample. One extracts fit parameters from each sample, and obtains the bootstrap distribution for each parameter. The resulting distribution is the best approximation one can make to the true distribution obtained by taking a large number of completely independent sets of N configurations each, as one would in applying cross validation to a huge ensemble. One course there are far too many $[N^N/N!\approx\exp(N)]$ possible bootstrap samples to actually perform the computation. Instead one estimates the bootstrap distribution by (what else) a Monte Carlo simulation. That is, one generates representative bootstrap samples by drawing N configurations at random from the ordinal set. Then from each sample one extracts a mass in the usual way. The bootstrap distribution for the $m_q=0.005$ $\tilde{\rho}$ mass is shown in Fig. 14(b). Note that it has a shape similar to the jackknife distribution (since the latter ensemble is basically a carefully chosen subset of the full bootstrap ensemble), but is sufficiently well populated that we need not use the usual mean and variance as estimates of the fit parameters and errors. Since the distribution is non-Gaussian in general, the median turns out to be more robust estimate of the central value than the simple average. Likewise we obtain the robust estimates of the errors by asking what values δ_+M and δ_-M from the median include the middle 63% of the distribution.

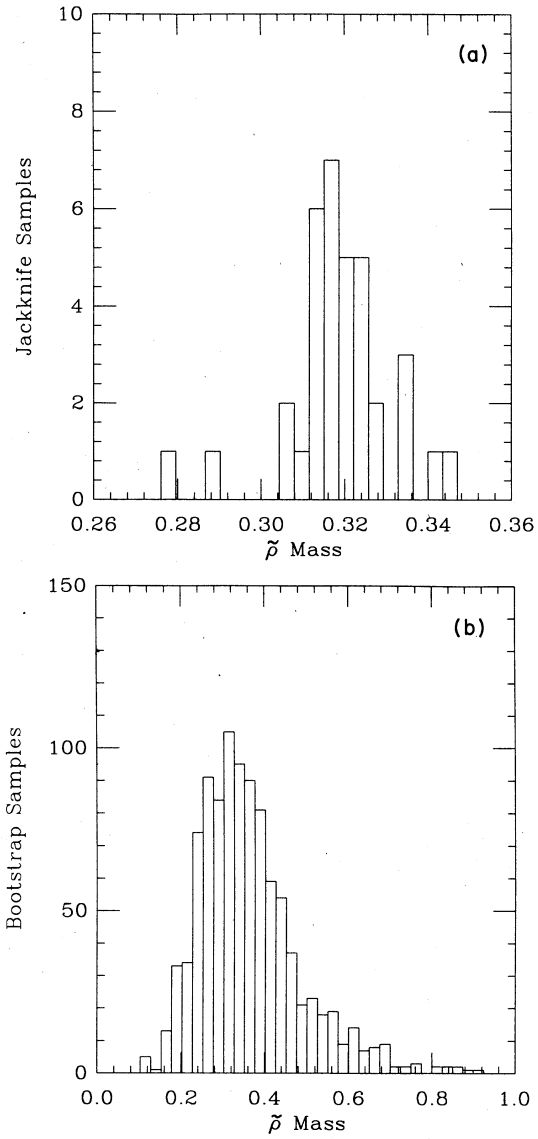

FIG. 14. Histogram of $m_{\tilde{\rho}}$ obtained from (a) 36 jackknife samples and (b) 1000 bootstrap samples of the $m_q=0.005$ zero momentum SF LNLT data.

In practice we find that the jackknife and bootstrap distributions for most observables look fairly Gaussian with our ensembles of only a few dozen configurations. In these cases the two error estimates agree. However, for those channels where the signal shows large fluctuations we definitely prefer to use bootstrap. In every case the errors we obtain using either jackknife or bootstrap methods bear little or no relation to naive error estimates.

[1]H. Hamber and G. Parisi, Phys. Rev. D **27**, 208 (1983).
[2]D. Weingarten, Phys. Lett. **109B**, 57 (1982).
[3]E. Marinari, G. Parisi, and C. Rebbi, Phys. Rev. Lett. **47**, 1795 (1981).
[4]R. Gupta, G. Guralnik, A. Patel, T. Warnock, and C. Zemach, Phys. Lett. **161B**, 352 (1985).
[5]K. C. Bowler, A. Hasenfratz, P. Hasenfratz, U. Heller, F. Karsch, R. D. Kenway, G. S. Pawley, and D. J. Wallace, Phys. Lett. B **179**, 375 (1987).
[6]S. A. Gottlieb, J. Kuti, D. Toussaint, A. D. Kennedy, S. Meyer, B. J. Pendleton, and R. L. Sugar, Phys. Rev. Lett. **55**, 1958 (1985).
[7]N. H. Christ and A. E. Terrano, Phys. Rev. Lett. **56**, 111 (1986).
[8]K. Bowler *et al.*, in *Lattice Gauge Theory '86*, proceedings of the NATO ARW Workshop, Brookhaven, 1986, edited by H. Satz, I. Harrity, and J. Potvin (Plenum, New York, 1987).
[9]For massive states the formula is given by M. Lüscher, Commun. Math. Phys. **104**, 177 (1986); for massless pions it is to be found in H. Leutwyler, Phys. Lett. B **189**, 197 (1987). The scattering amplitudes of the quenched approximation (glueball exchange) must be used in these formulas.
[10]A. Morel and J. P. Rodrigues, Nucl. Phys. **B247**, 44 (1984).
[11]G. W. Kilcup, S. R. Sharpe, R. Gupta, G. Guralnik, A. Patel, and T. Warnock, Phys. Lett. **164B**, 347 (1985).
[12]G. W. Kilcup and S. R. Sharpe, Nucl. Phys. **B283**, 493 (1987).
[13]Lattice charge conjugation differs in general from continuum charge conjugation. Thus particles with the same charge-conjugation parity in the continuum need not have the same lattice charge-conjugation parity. For the explicit expression relating the two parities, see Ref. 12.
[14]R. Gupta, G. W. Kilcup, and S. R. Sharpe, Phys. Lett. **147B**, 339 (1984).
[15]O. Martin and A. Patel, Phys. Lett. B **174**, 94 (1986).
[16]S. Gottlieb, P. B. Mackenzie, H. B. Thacker, and D. Weingarten, Nucl. Phys. **B263**, 704 (1986).
[17]B. Efron, Ann. Stat. 7, 1 (1979).
[18]There is always the possibility that the true chiral behavior sets in at much smaller masses and that the observed proportionality of $m_\pi{}^2$ to m_q is a conspiracy.
[19]A Morel, Report No. SACLAY-PhT/87-020, 1987 (unpublished).
[20]A. Billoire, R. Lacaze, E. Marinari, and A. Morel, Nucl. Phys. **B271**, 461 (1986).
[21]K. H. Mütter, in *Lattice Gauge Theory '86* (Ref. 8).
[22]J. Mandula and M. Ogilvie, Phys. Lett. B **185**, 127 (1987).
[23]H. Hamber, Phys. Lett. B **178**, 277 (1986).
[24]K. C. Bowler, D. L. Chalmers, R. D. Kenway, G. S. Pawley, and D. Rowek, Nucl. Phys. **B284**, 299 (1987).
[25]D. Barkai, K. J. M. Moriarty, and C. Rebbi, Phys. Lett. **156B**, 385 (1985).
[26]S. Ono, Phys. Rev. D **17**, 888 (1978).
[27]S. Itoh, Y. Iwasaki, and T. Yoshie, Phys. Lett. B **183**, 351 (1987).
[28]R. Jaffe and C. L. Korpa, Commun. Nucl. Part. Phys. **17**, 163 (1987).
[29]S. Capstick and N. Isgur, Phys. Rev. D **34**, 2809 (1986); S. Godfrey and N. Isgur, *ibid.* **32**, 189 (1985).
[30]Nathan Isgur (private communication).